PHOTOPRODUCTION OF JETS AND PROMPT PHOTONS AT HERA*

J. CVACH
Centre for Particle Physics, Institute of Physics AS CR
Na Slovance 2,
Prague 8, CZ-182 21, Czech Republic
E-mail: cvach@fzu.cz

Recent measurements of jet and prompt photon production at HERA are reviewed. The results are compared to NLO QCD calculations which describe the data well except in extreme regions of phase space. Studies of the inclusive single jet cross section provide very accurate value of α_s.

1. Introduction

At the positron–proton HERA collider positrons[a] of energy 27.6 GeV collide with protons with energy 820 (until 1997) or 920 GeV. The positrons are the source of quasi-real photons which interact with the protons. We usually call their interactions photoproduction at HERA if the photon virtuality $Q^2 < 1$ GeV^2. Scattered positrons at higher virtualities are detected in the main detector and lead to processes which are called deep inelastic scattering. Photoproduction represents the dominant hard scattering process and provides, therefore, the most accurate results in a large kinematic range. In the lowest order of the perturbative series expansion in α_s, a quasi-real photon interacts with a parton from the proton directly (Fig. 1a) or as resolved (Fig. 1b) via one of its partons generated in a hadronic fluctuation. Due to the QCD radiation and fragmentation processes, the partons appear as collimated jets of particles accompanied in general by the proton remnant and, in the case of resolved processes, by the photon

*This work is supported by the Ministry of Education of the Czech Republic under the projects INGO-LA116/2000 and LN00A006.
[a]We use positron for the HERA lepton beam where electrons are used as well. As the electron data sample has significantly smaller luminosity we mention electrons explicitly where it is relevant.

remnant and by particles resulting from a possible remnant-remnant interaction, also called the underlying event. The cross sections for direct and

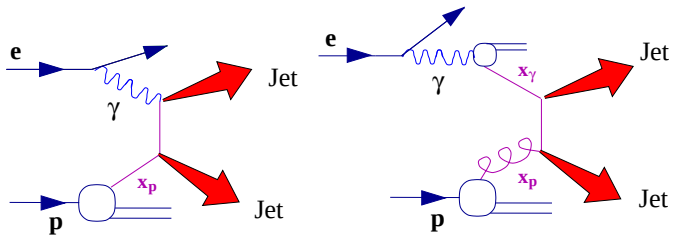

Figure 1. Example LO QCD diagrams for jet-jet photoproduction in direct (a) and resolved (b) photon interactions.

resolved photon interactions are given to LO by:

$$\sigma_{\rm dir}^{ep\to {\rm ejetjet}(\gamma)X} = \sum_j f_{i/p} \otimes \hat{\sigma}_{ej\to {\rm jetjet}(\gamma)}$$

and for the resolved photon interaction by:

$$\sigma_{\rm res}^{ep\to {\rm ejetjet}(\gamma)X} = \sum_{i,j} f_{\gamma/e} \otimes f_{i/\gamma} \otimes f_{j/p} \otimes \hat{\sigma}_{ij\to {\rm jetjet}(\gamma)}\,,$$

where $f_{k/a}$ is the parton density function (PDF) for parton k in the particle $a = \gamma, p$ and $f_{\gamma/e}$ is the photon flux in the positron given by the equivalent photon approximation, $\hat{\sigma}_{ej}$ is the cross section for positron–quark scattering using the exact matrix element (which is also valid in the NLO case) and $\hat{\sigma}_{ij}$ is the cross section for parton–parton scattering. PDFs depend on the factorization scale μ_f and the cross sections $\hat{\sigma}$ on the renormalization scale μ_r via α_s. Here both scales are set to be equal.

The new HERA results on jet photoproduction are based on luminosities of several tens of pb^{-1}. They allow comparisons to the NLO calculations up to higher jet E_T and in a more differential way. Studying high E_T jets has the advantage that the hadronisation of the parton from the hard scattering influences the jet less. Also, the impact of soft processes from the proton–photon remnant interaction are less important. Having achieved good agreement with the NLO calculations, data are used to check different parametrization of the PDFs of the photon, which are mostly known from F_2^γ measurements at LEP. HERA data are unique due to the high sensitivity to the gluon density in the photon via the dominant boson–gluon

fusion process. The sensitivity to the PDFs is high in the region where the difference between the rapidities of both jets is small. In contrast, the region with large jet rapidity difference is sensitive to the form of the matrix element.

We will first present results on single jet inclusive cross section measurements which provide a very accurate value of α_s. Then we review the results on dijet inclusive cross sections. From the four-momenta of both jets, the fraction of the photon momentum carried by the interacting parton $x_\gamma^{\rm jet}$ can be estimated. This quantity is used to separate direct and resolved events and to investigate the dynamics of these classes separately. Finally, new data on direct photon production are compared to NLO QCD calculations.

Since most of the results use a similar experimental procedure, we shall summarize here their main features:

(a) $Q^2 < 1$ GeV^2, $0.1 < y < 0.9$ (H1), $0.2 < y < 0.85$ (ZEUS).
(b) Jets were obtained using the inclusive k_t algorithm[1].
(c) Data were corrected for detector effects using two of three MC event generators, PYTHIA[2] and PHOJET[3], which both use LUND strings for fragmentation and HERWIG[4] with its cluster fragmentation scheme. Soft processes are modeled in PYTHIA as Multiple Interactions between the proton and photon remnants, PHOJET uses the Dual Parton Model[5] and HERWIG adds an adjustable fraction of the soft underlying events.
(d) The dominant systematic errors come from two sources: uncertainty in the knowledge of the energy scale in the hadron calorimeter causes errors of 20% at low E_T which drop below 10% at high E_T and model dependence of the detector corrections which causes errors below 10%.

For the comparison of data with NLO predictions the following calculations are used:

(a) NLO weighted parton MC of Frixione[6] using GRV-HO[7] for the photon and CTEQ5M[8] for the proton PDF as the standard parametrization. To test the dependence of the calculation on the PDF parametrization, other choices were used such as MRST99 and CVTEQ5HJ for the proton and AFG-HO for the photon.
(b) The program of Klasen, Kleinwort and Kramer[9] using the phase space (PS) slicing method to separate the infrared and mass singular

phase space region.

(c) The program of Fontannaz, Guillet and Heinrich[10] for isolated prompt photon production combines the PS slicing and subtraction methods. It uses AFG for the photon and MRST2 for the proton PDFs.

(d) As the calculations are done for partons, the main uncertainty comes from the hadronisation correction and decreases from 20% for low E_T to less than 10% at high E_T. The renormalization and factorization scale uncertainty is below 10%.

Experimental data are displayed in figures with the inner error bars denoting the statistical error. Systematic errors without the uncertainty due to the jet energy scale are added in quadrature with the statistical error and shown as the outer error bars. The uncertainty due to the jet energy scale is shown separately as a shaded band.

The dominant partonic subprocesses responsible for jet production at HERA are $\gamma g_p \to q\bar{q}$ and $q_\gamma g_p \to qg$. The kinematics of these two-to-two subprocesses are such that the majority of jets in the region of jet pseudorapidity $\eta^{\rm jet} < 0$ are predicted to originate from outgoing quarks while the fraction of gluon-initiated jets increases as $\eta^{\rm jet}$ increases[11]. Therefore, the experimental investigation of jet properties as a function of jet pseudorapidities allows the study of the characteristics of quark- and gluon-initiated jets. To distinguish between both types of jets, jet shapes and mean subjet multiplicities using the k_t-cluster algorithm were used as an analyser. The jets become broader and the mean subjet multiplicity increases for final-state gluon-initiated jets. The use of simultaneous cuts on the jet shapes and subjet multiplicity allowed the definition of enriched samples of quark- ("thin") and gluon- ("thick") initiated jets.

The distribution of the angle between the jet-jet axis and the beam direction in the dijet centre-of-mass system $\cos\theta^*$ is sensitive to the spin J of the exchanged particle $d\sigma/d\cos\theta^* \sim (1 - |\cos\theta^*|)^{-2J}$ as $|\cos\theta^*| \to 1$. In the case of direct photon interactions the contributing processes in LO QCD are $\gamma q(\bar{q}) \to gq(\bar{q})$ and $\gamma g \to q\bar{q}$ which involve quark exchange in the s, t and u channels. In the case of resolved photon interactions, the contributing processes $qg \to qg$, $qq' \to qq'$, $gq \to gq, \ldots$ involve gluon exchange. The study of the angular distribution of dijet events thus provides a handle for the investigation of the underlying parton dynamics[12].

2. Single jet production and α_s

The new measurements from H1[13] cover an extended range of jet transverse energies between 5 and 75 GeV. For $E_T^{\rm jet} \geq 21$ GeV, the hadronisation corrections to the NLO QCD calculation only slightly improve the agreement with data, whereas for $5 < E_T^{\rm jet} < 21$ GeV good agreement can only be obtained by applying them. The NLO predictions are in agreement with the $d\sigma/d\eta^{\rm jet}$ by measurements in different $E_T^{\rm jet}$ bins except in the lowest range $5 < E_T^{\rm jet} < 12$ GeV (see Fig. 2). The data seem to indicate a rise of the cross section with increasing $\eta^{\rm jet}$ which is faster than in the theoretical predictions. Inadequacy of the photon PDFs in this kinematic range or the

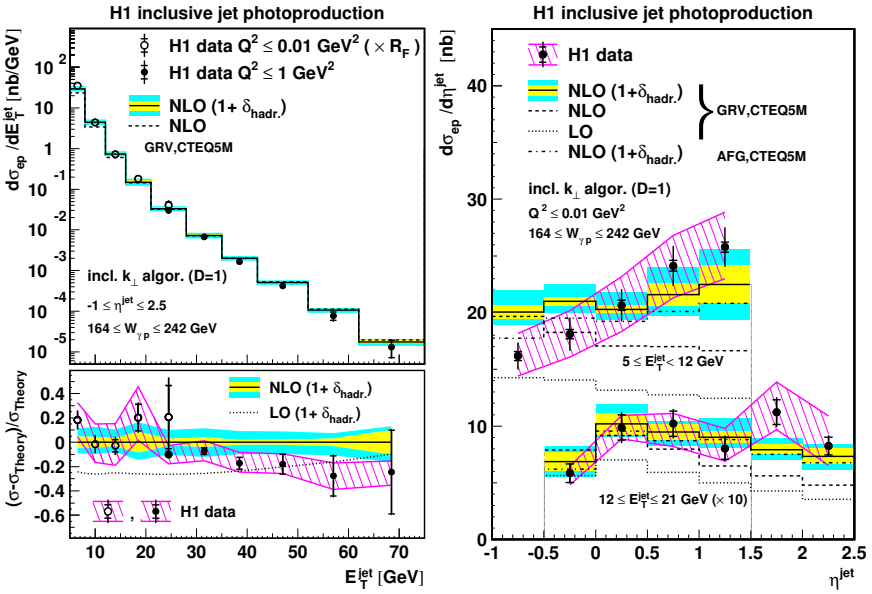

Figure 2. Differential e^+p cross section for inclusive jet production as a function of (a) $E_T^{\rm jet}$ integrated over $-1 < \eta^{\rm jet} < 2.5$. At the bottom of the figure, the relative difference between data or LO QCD and the NLO calculations, including hadronisation correction, are shown. (b) $\eta^{\rm jet}$ integrated over the two lowest $E_T^{\rm jet}$ ranges. The data are compared with LO and NLO QCD predictions obtained by using GRV or AFG photon PDFs and CTEQ5M proton PDFs.

absence of higher order corrections beyond NLO may be responsible.

ZEUS measured[14] the inclusive jet cross section as a function of $E_T^{\rm jet}$ in the range between 17 and 95 GeV. No significant deviation with respect to QCD NLO calculation was observed up to the highest scale studied. The

measured cross section $d\sigma/dE_T^{\rm jet}$ was used to determine $\alpha_s(M_Z)$ using the method presented previously[15]. The $\alpha_s(M_Z)$ dependence of the predicted

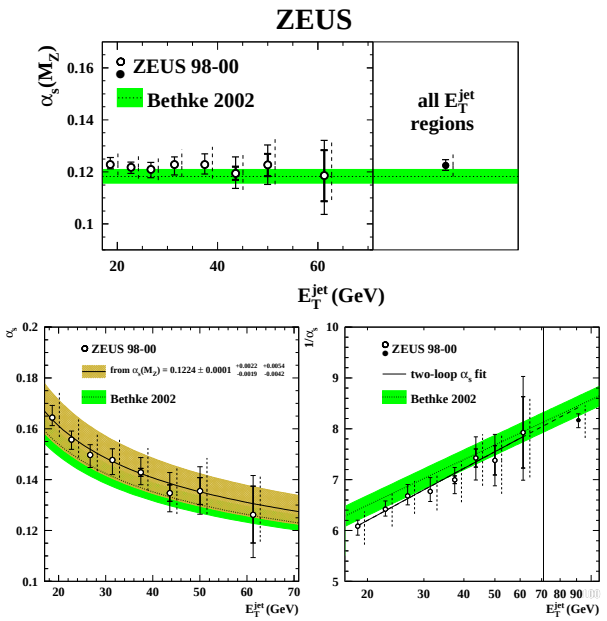

Figure 3. (top) The $\alpha_s(M_Z)$ values determined from the QCD fit to the measured $d\sigma/dE_T^{\rm jet}$ values in different $E_T^{\rm jet}$ regions (open circles) and the combined value. (lower left) The $\alpha_s(E_T)$ values determined from the QCD fit of the measured $d\sigma/dE_T^{\rm jet}$ values as a function of $E_T^{\rm jet}$ (open circles). The solid line represents the prediction of the renormalization group equation; the light shaded area displays its uncertainty. (lower right) The $1/\alpha_s(E_T)$ values as a function of $E_T^{\rm jet}$ (open circles). The solid line represents the result of the two-loop α_s fit to the measured values, the dashed line the extrapolation of the fit to $E_T^{\rm jet} = M_Z$. The point plotted at $E_T^{\rm jet} = M_Z$ represents the inverse of the combined value from (top).

$d\sigma/dE_T^{\rm jet}$ in each bin of $E_T^{\rm jet}$ was parametrised according to

$$[d\sigma/dE_T^{\rm jet}(\alpha_s(M_Z))]_i = C_1^i \alpha_s(M_Z) + C_2^i \alpha_s^2(M_Z)$$

where C_1^i and C_2^i are constants, by using the NLO QCD calculations corrected for hadronisation effects. Finally, a value of $\alpha_s(M_Z)$ was determined in each bin of the measured cross section as well as from all data by a χ^2 fit. The value of $\alpha_s(M_Z)$ is

$$\alpha_s(M_Z) = 0.1224 \pm 0.0001(\text{stat.})^{+0.0022}_{-0.0019}(\text{exp.})^{+0.0054}_{-0.0042}(\text{th.})\,.$$

This value of $\alpha_s(M_Z)$ is consistent with the current world average[16] of 0.1183 ± 0.0027. The largest contribution to the experimental uncertainty comes from the jet energy scale and amounts to $\pm 1.5\%$. The QCD prediction for the energy scale dependence of α_s was tested by determining α_s from $d\sigma/dE_T^{\rm jet}$ at different $E_T^{\rm jet}$ values. The measured $\alpha_s(E_T)$ values are shown in Fig. 3 and are in good agreement with the predicted running of the strong coupling constant over a large range of $E_T^{\rm jet}$.

The cross section $d\sigma/d\eta^{\rm jet}$ is presented in Fig. 4a for samples of "thick" and "thin" jets separated according to the method explained in Section 1. The measured cross sections for the two samples of jets exhibit different behaviour: the $\eta^{\rm jet}$ distribution for "thick" jets peaks at $\eta^{\rm jet} \sim 2$, whereas the distribution from "thin" jets peaks at $\eta^{\rm jet} \sim 0.7$. The same selection methods has been applied to the jets of hadrons in the Monte Carlo samples (PYTHIA, HERWIG and PYTHIA MI). The MC predictions provide a good description of the shape of the "thin"-jet data distribution. From

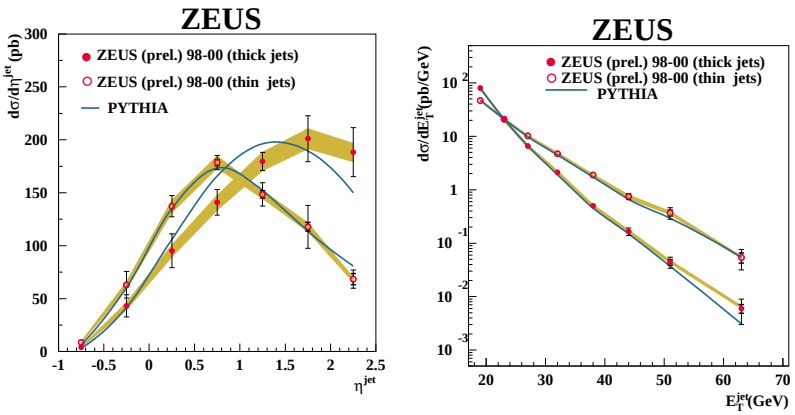

Figure 4. (a) Differential ep cross section $d\sigma/d\eta^{\rm jet}$ for inclusive jet production integrated over $E_T^{\rm jet} > 17$ GeV for "thick" and "thin" jets. (b) Differential $d\sigma/dE_T^{\rm jet}$ cross section integrated over $-1 < \eta^{\rm jet} < 2.5$. The PYTHIA prediction normalised to the total cross section is shown for comparison.

the calculation of PYTHIA the sample of "thick" jets is predicted to contain 52% (16%) of events resulting from $gq(gg)$ subprocesses in the final state. The sample of "thin" jets contains 65% (33%) of events from $qq(qg)$ subprocesses. The cross section $d\sigma/dE_T^{\rm jet}$ is shown separately for "thick" and "thin" jet samples. The "thin" jet sample exhibits a harder spectrum than the "thick"-jet sample.

3. Dijet production and photon structure

Requiring at least two jets per event makes possible the determination of the distribution of fractional parton momentum $x_p(x_\gamma)$ in the proton (photon) and of the centre-of-mass scattering angle $\cos\theta^*$ of the partons using two-to-two particle scattering kinematics via the expressions:

$$x_p^{\rm obs} = \sum_{i=1}^{2} E_T^{{\rm jet}i} \exp(\eta^{{\rm jet}i})/2E_p, \qquad x_\gamma^{\rm obs} = \sum_{i=1}^{2} E_T^{{\rm jet}i} \exp(-\eta^{{\rm jet}i})/2E_\gamma,$$

$$\cos\theta^* = \tanh(\eta^{\rm jet1} - \eta^{\rm jet2})/2\,.$$

Both experiments have published new cross sections from photoproduction. The H1 experiment[17] concentrated on double differential x_p and x_γ measurements. The data at the highest $x_p \sim 0.6$ are sensitive to the gluon density of the proton, which contributes almost 40% of the cross section. The $d\sigma/dx_\gamma$ cross sections are presented for different regions of the variables x_p and $E_{T,\rm max}^{\rm jet}(= E_T^{\rm jet1}$, the transverse energy of the highest E_T jet). The data (Fig. 5 left) are compared to NLO calculations with two different

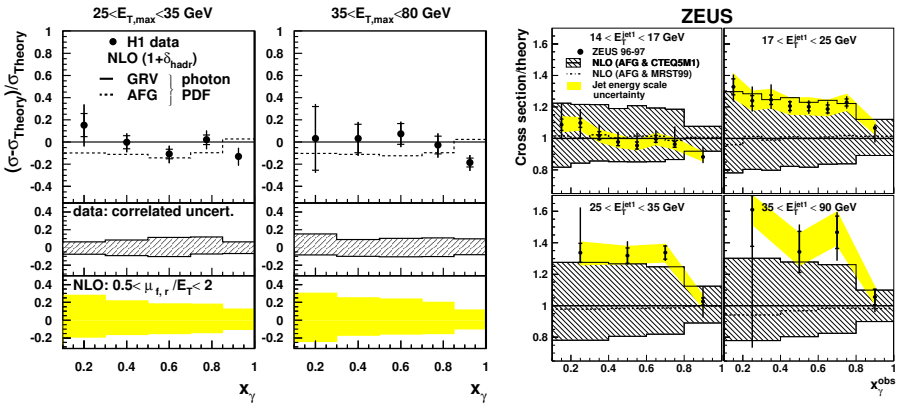

Figure 5. (left) The x_γ dependence of the relative difference of the measured H1 dijet cross sections to the NLO prediction with hadronisation corrections. The two figures show the relative difference for two $E_{T,\rm max}$ bins. The error due to the uncertainty in the calorimeter energy scale is shown in the middle. The band in the lower plot shows the renormalization and factorization scale uncertainties. (right) Ratio of cross sections from the ZEUS experiment to the NLO prediction using AFG-HO and CTEQ5M1 as the photon and proton PDFs, with the scale set to $E_T/2$. The theoretical uncertainty is shown as a hatched band.

parameterizations of the photon structure. The prediction describes the data well. The conclusion of the analysis is that the data do not require

significant changes in the parameterizations of the PDFs but do provide useful further constraints.

ZEUS published[18] dijet cross sections as a function of $E_T^{\rm jet1}$ in different regions of the pseudorapidity of the two jets for $x_\gamma^{\rm obs} > 0.75$ and $x_\gamma^{\rm obs} < 0.75$. In general, the description of the data by NLO predictions is reasonable except when both jets are produced in the range $1 < \eta^{\rm jet} < 2.4$. Here the NLO prediction lies below the data at low transverse energy. Similarly to H1, ZEUS tests the current parametrization of the photon PDFs in different bins of $E_T^{\rm jet1}$ (see Fig. 5 right). The predictions using the GRV-HO parametrization agree with the data in the region of lowest transverse energy, but are below the data for the higher $E_T^{\rm jet1}$ bins. The predictions using AGF-HO are similar in shape to those using GRV-HO but are (10-15)% lower.

To improve the understanding of the cross section in different regions of transverse energy, the sensitivity to the value of the transverse energy cut on the second jet has been studied. Starting at a minimum of 11 GeV, the cut on $E_T^{\rm jet2}$ was raised in both data and theory for the region $25 < E_T^{\rm jet1} < 35$ GeV. The data fall less steeply with the increasing transverse energy than do the NLO QCD predictions and show sensitivity to the parton densities of the photon. Neither the AFG-HO nor the GRV-HO parametrization, convoluted with the NLO matrix element, fully describe the data. The data and NLO calculation cross each other at $E_T^{\rm jet2} \sim 15$ GeV which is the cut used in the H1 analysis. This may explain why in the interval $25 < E_T^{\rm jet1} < 35$ GeV shown in Fig. 5 left, H1 observes good agreement with the NLO QCD calculation with both photon PDFs, as H1 uses a higher cut $E_T^{\rm jet2} > 15$ GeV than ZEUS.

ZEUS defined dijet data samples of "thick-thick", "thin-thin" and "thick-thin" events according to the criteria mentioned in Section 1. The differential dijet cross section as a function of $\cos\theta^*$ was measured[12] in the range of $|\cos\theta^*| < 0.8$ for dijet invariant mass $M^{\rm jj} > 52$ GeV. The region of phase space in the $(M^{\rm jj}, \cos\theta^*)$ plane was chosen in order to minimise the biases introduced by selecting jets with $E_T^{\rm jet1} > 17$ GeV and $E_T^{\rm jet2} > 14$ GeV. Fig. 6a shows the measured dijet cross section as a function of $\cos\theta^*_{\rm thick}$. Calculations using PYTHIA and HERWIG give a good description of the shape of the measured cross section. The measured and predicted cross sections were normalised so as to have a value of unity at $\cos\theta^*_{\rm thick} = 0.1$. The prediction of HERWIG for the partonic content is 41% of qg, 6% of gg and 53% of qq subprocesses. The observed asymmetry is adequately reproduced by the calculation and is understood in terms of the dominance

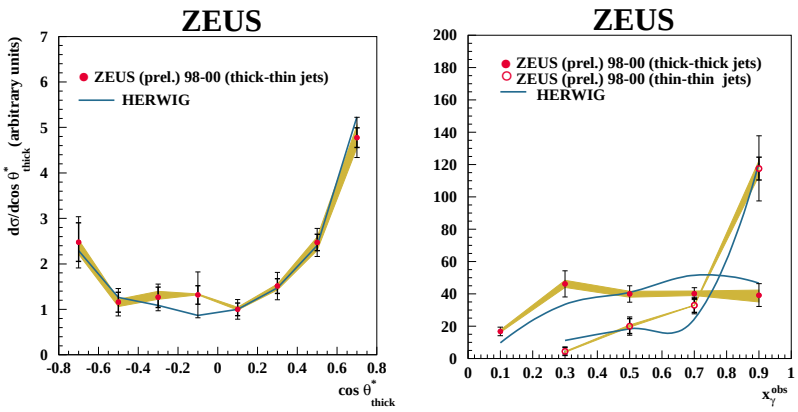

Figure 6. Differential ep cross section (a) $d\sigma/d\cos\theta^*_{\rm thick}$ for dijet production. The cross section is for dijet events with "thick–thin" selection. The HERWIG prediction is normalised to data at $\cos\theta^*_{\rm thick} = 0.1$. (b) $d\sigma/dx_\gamma^{\rm obs}$ for dijet production with "thick–thick" (black dots) and "thin–thin" (open circles) jet selection. The HERWIG prediction is normalised to the total measured cross section. Cross sections in (a) and (b) are integrated over $E_T^{\rm jet1} > 17$ GeV, $E_T^{\rm jet2} > 14$ GeV and $-1 < \eta^{\rm jet} < 2.5$.

of the resolved subprocess $q_\gamma g_p \to qg$. The $\cos\theta^*_{\rm thick}$ distribution is asymmetric due to the different dominant diagrams in the different kinematic regions.

As the virtuality of the photon increases, the photon structure gradually changes. Whereas for quasi-real photons, the PDF approach is an indispensable theoretical tool, for $Q^2 \gg \Lambda^2_{\rm QCD}$ the data can be analysed using perturbative calculations of the direct process. However, the resolved photon concept is still useful phenomenologically provided the photon virtuality remains smaller than a measure of the hardness of the process, e.g. $E_T^{\rm jet}$. In the new analysis[19] from H1 of electroproduction of dijets at $2 < Q^2 < 80\,{\rm GeV}^2$, triple differential dijet cross sections were analysed within several theoretical approaches, differing in the way higher order QCD effects were taken into account. The NLO direct calculation of JETVIP[20] is shown in Fig. 7 by a broken line and is in marked disagreement with the data in the region of small Q^2, small $E_T^{\rm jet}$ and small x_γ. JETVIP is the only NLO program which calculates also the NLO resolved photon contribution. The sum of both cross sections direct + resolved, is shown by the full line in Fig. 7. The agreement between data and calculations improves, but is still not satisfactory. The conclusion is that the data show clear evidence of the need for $\alpha\alpha_s^3$ and higher order terms in the theory. The best description of

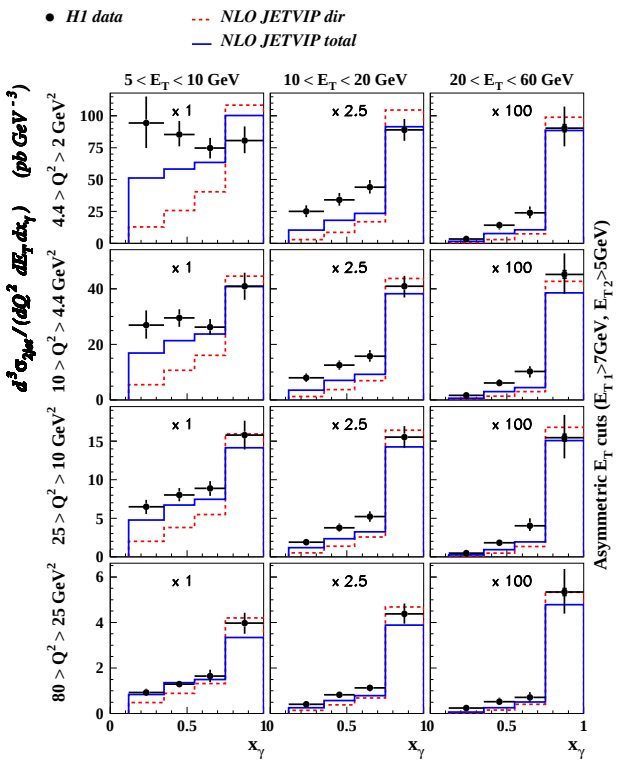

Figure 7. Triple differential dijet cross section $d^3\sigma/dQ^2dE_Tdx_\gamma$ for the H1 data depicted by points compared to the prediction of JETVIP NLO calculations corrected for hadronisation effects. The dashed line shows the NLO direct cross section, the full line the sum of NLO direct and NLO resolved contributions.

the data (not shown here) is achieved with the LO HERWIG generator with the inclusion of longitudinally polarised resolved photon and initial and final state parton showers as an effective approximation to higher order QCD processes.

4. Prompt photon production

Prompt photons are produced in direct and resolved interactions when a hard photon emerges instead of a gluon jet. Since the properties of hard photons can be more accurately measured than those of a jet, prompt photons are expected to allow cleaner tests of parton dynamics. Two obstacles

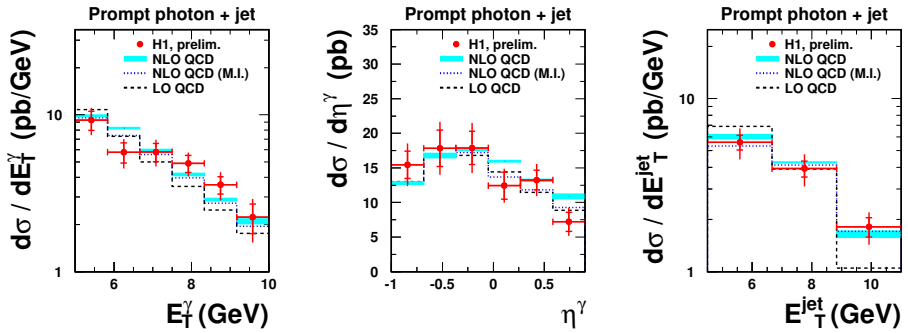

Figure 8. Prompt photon differential cross sections as a function of E_T^γ, η^γ and $\eta^{\rm jet}$. The data are compared to LO (dashed) and NLO calculations. The error bands show the effect of a variation of the renormalization and factorization scales in the NLO calculations from $0.5E_T^\gamma$ to $2E_T^\gamma$. Dotted line shows the NLO result corrected for multiple interaction effects using PYTHIA.

make these advantages less clear: prompt photons are born in an environment of copious production of photons from π^0 decays and their production cross section is a factor of α/α_s smaller than that of gluon jets. H1 has presented new results[21] on the photoproduction of isolated prompt photons, both inclusively and in association with jets. The cross sections are given for transverse photon energies and pseudorapidities of $5 < E_T^\gamma < 10$ GeV, $-1 < \eta^\gamma < 0.9$ and for jets in the range $E_T^{\rm jet} > 4.5$ GeV, $-1 < \eta^{\rm jet} < 2.3$. The cross sections for a prompt photon with a jet are presented in Fig. 8 and compared to NLO calculations[10]. The NLO corrections are substantial and lead to a good description of the data. Taking into account the multiple interaction effects (PYTHIA) improves the data description in particular at $\eta^\gamma > 0$ and $x_\gamma < 0.5$. The NLO prediction is not corrected for hadronisation effect. The H1 cross sections were also compared to the measurements[22] of the ZEUS Collaboration. The results are consistent but the H1 data are somewhat lower at small η^γ where the ZEUS data appear to exceed the NLO calculation.

5. Conclusions

The H1 and ZEUS Collaborations have provided accurate measurements of jet and prompt photon cross sections at the lowest photon virtualities. Data were compared to several NLO calculations which agree very well at large values of the hard scale (usually $E_T^{\rm jet}$). The QCD analysis of inclusive

jet $d\sigma/dE_T^{\rm jet}$ cross sections leads to accurate value of α_s which are in good agreement with the world average. At the edges of the phase space of the current measurements (low $E_T^{\rm jet}$, large $\eta^{\rm jet}$), especially when cross sections are presented in a multi-differential way, differences between data and NLO calculations become significant. Data provide constraints on the photon PDF.

Acknowledgments

I am indebted to all members of the H1 and ZEUS collaborations who contributed to the results. Especially, I would like to thank to my colleagues J. Chýla, T. Greenshaw, G. Grindhammer, T. Kluge, R. Lemrani, P. Van Michelen, M. R. Sutton, J. Terrón and A. Valkárová who helped me with the preparation of this review. I would like to thank the organizers of the Ringberg workshop for preparing a stimulating meeting.

References

1. S. D. Ellis and D. E. Soper, *Rev. Phys.* **D48**, 3160 (1993).
2. T. Sjöstrand, *Comput. Phys. Commun.* **82**, 14 (1994).
3. R. Engel, *Z. Phys.* **C66**, 203 (1995).
4. G. Marchesini et al., *Comput. Phys. Commun.* **67**, 465 (1992).
5. A. Capella et al., *Phys. Rept.* **236**, 225 (1994).
6. S. Frixione, *Nucl. Phys.* **B507**, 295 (1997).
7. M. Glück, E. Reya and A. Vogt, *Phys. Rev.* **D45**, 9863 (1992).
8. H. L. Lai et al., [CTEQ Collaboration], *Eur. Phys. J.* **C12**, 375 (2000).
9. M. Klasen, T. Kleinwort and G. Kramer *Eur. Phys. J. Direct* **C1**, 1 (1998).
10. M. Fontannaz, J. P. Guillet and G. Heinrich, *Eur. Phys. J.* **C21**, 303 (2001).
11. J. Breitweg et al., *Eur. Phys. J.* **C2**, 61 (1998).
12. ZEUS Collaboration, Substructure dependence of jet cross section at HERA, Abstract 518, IECHEP Aachen, Germany, 2003.
13. C. Adloff et al., DESY 02-225, hep-ex/0302034.
14. S. Chekanov et al., *Phys. Lett.* **B560**, 7 (2003).
15. J. Breitweg et al., *Phys. Lett.* **B507**, 70 (2001);
    S. Chekanov et al., *Phys. Lett.* **B547**, 164 (2002).
16. S. Bethke, *Nucl. Phys. Proc. Suppl.* **121**, 4 (2003).
17. C. Adloff et al., *Eur. Phys. J.* **C25**, 13 (2002).
18. S. Chekanov et al., *Eur. Phys. J.* **C23**, 615 (2002).
19. A. Aktas et al., H1 Collaboration, Measurement and QCD analysis of dijet production at low Q^2 at HERA, to be published in *Eur. Phys. J.*
20. B. Pötter, *Comp. Phys. Commun.* **133**, 105 (2001).
21. H1 Collaboration, Measurement of Prompt Photon Production in γp Interactions, Abstract 093, IECHEP Aachen, Germany, 2003.
22. J. Breitweg et al., *Phys. Lett.* **B472**, 175 (2000).